https://dx.doi.org/10.1016/j.jclepro.2023.139634

Drying Behavior Modeling of Bitumen Emulsion-based Cold In-place Recycling Pavement Considering Heat-moisture Coupling Effects

Jiwang Jiang[1, *], Jingling Wang[1], Zili Zhao[1], Fujian Ni[1], Duo Xu[1], Zhu Zhang[1], Zhen Leng[2, *]

[1] School of Transportation, Southeast University, Nanjing, Jiangsu, China, 211189
[2] Department of Civil and Environmental Engineering, The Hong Kong Polytechnic University, Hung Hom, Kowloon, Hong Kong
[*] Corresponding authors. Email: jiang_jiwang@seu.edu.cn (J. Jiang); zhen.leng@polyu.edu.hk (Z. Leng)

ABSTRACT

Bitumen Emulsion-based Cold In-place Recycling (BE-CIR) pavement has been widely applied for its energy-saving and environmental friendliness. BE-CIR is manufactured at ambient temperature and requires a specific drying duration to develop sufficient strength before overlay placement. However, it is challenging to characterize the drying behavior of BE-CIR pavement due to the complex field curing environments and strength formation process. Hence, this research aims to develop a drying behavior model of BE-CIR pavement considering the heat-moisture coupling effects, which can help optimize the timing for overlay placement under different curing environments. Numerical models of mixture and pavement were established based on the heat and mass transfer theories. Actual temperature and humidity data obtained from laboratory tests and field monitoring were used for model calibration and validation. Time-variable coefficient and depth correction coefficient developed based on functional relationships of physical parameters were proposed to calibrate the model. The finite element calculation results indicated that the calibrated model could effectively simulate the drying behavior of BE-CIR pavement under natural curing environments. Two typical working conditions based on natural pavement curing environments were simulated. The calculation results suggested that the curing time required to reach moisture equilibrium was 120 hours at medium temperature and high humidity and 50 hours at low temperature and medium humidity, both higher than the measured 30 hours at high temperature and low humidity.

Keywords: Bitumen emulsion; Cold in-place recycling; Drying behavior; Numerical simulation; Heat-moisture coupling effects

1 INTRODUCTION

Bitumen Emulsion-based Cold In-place Recycling (BE-CIR) pavement is a green technology for asphalt pavement recycling (Xiao et al., 2018). In the BE-CIR pavement recycling process, crushed old pavement, i.e., aggregates coated with old asphalt, are used as the aggregate source (Gu et al., 2019). Bitumen emulsion is used as the main binder, while non-organic additives, such as Portland cement, are incorporated to obtain high early-stage strength, which allows traffic to be opened earlier (Modarres et al., 2014). Compared to hot recycling pavement, BE-CIR pavement offers significant advantages in terms of energy consumption, economic costs, and environmental protection (Alkins et al., 2008). This is attributed to the 100% utilization of reclaimed asphalt pavement (RAP) and the elimination of heating processes during construction. Nonetheless, BE-CIR is commonly used as a base course material with an additional overlay placed on top due to its relatively weak mechanical properties.

BE-CIR mixture is a visco-elasto-plastic material with complex composition. After rehabilitation and compaction, the BE-CIR mixture is cured under the environmental contexts of ambient temperature and relative humidity (RH). The development of bitumen films containing fine aggregates, non-organic additives, and hydration products during curing is the main contributor to the strength formation of the mixture, resulting from multiple physical and chemical interactions, including emulsion breaking and non-organic additives hydration. Bitumen droplets dispersed in emulsion gradually flocculate and coalesce as the moisture evaporates. This process may continue for more than 28 days and contributes to the long-term mechanical properties of BE-CIR pavement (Miljković and Radenberg, 2015). Hydration reaction between non-organic additives and water can increase alkalinity to change the chemical stability of bitumen emulsion, while hydration products dispersed in bitumen film can increase the viscosity and deformation resistance of BE-CIR (Du, 2014). The curing process can be characterized by water content, which decreases until reaching equilibrium with the environment, with a final water content of approximately 1% by mass of the mixture (Graziani et al., 2016). A portion of this water is trapped in the bitumen film, deteriorating the mixture's cohesive and adhesive properties (Khan et al., 2016). To evaluate the effect of initial water content on pavement performance and the curing degree characterized by mechanical properties, a series of strength indexes or stiffness indexes, including indirect tensile strength, failure tensile strain, and stiffness modulus, were tested (Ouyang et al., 2019). In fact, the effect of water on the mechanical properties and performance of BE-CIR pavement starts from compaction (Gao et al., 2014). Evidently, the presence and transfer of moisture are strongly related to the development of the mechanical properties of the mixture.

Water in newly constructed BE-CIR pavement mainly comes from bitumen emulsion, which contains 25-60% water, and extra water, which accounts for around 2% by mass of the mixture (Flores et al., 2020). Water in bitumen emulsion is used to disperse bitumen droplets for long-term preservation. Due to the lubricating effect, extra water is added in the recycling process to pave and compact the BE-CIR mixture instead of heating and to ensure that bitumen film can coat the aggregate surface entirely and uniformly. To predict the development pattern of mechanical properties and to clarify the strength formation process, research on drying behavior in BE-CIR pavement is essential. As the essential feature of drying behavior, moisture migration is a process of water transfer and phase transition in porous media under the heat-moisture coupling interaction. Fig. 1 illustrates the process of moisture migration in BE-CIR pavement. The mechanism of moisture migration in asphalt pavement includes surface infiltration, capillary rise, and diffusion (Arambula et al., 2010). In the initial curing phase of BE-CIR pavement, diffusion dominates the moisture migration, consisting of gaseous water molecules diffusion and the liquid water molecules evaporation, a phase transition process in which water molecules move away from the surface of the liquid under the action of Brownian motion. After compaction, liquid water evaporates into the gaseous phase, which moves to a lower RH environment following Fick's law. Ultimately, the water content in the BE-CIR mixture is reduced to equilibrium. This process is affected by a combination of internal factors and environmental factors. Internal factors include bitumen emulsion breaking rate, ionic properties of bitumen emulsion, additives interference, micro-void structure, and so on. External factors include ambient temperature, RH, wind speed, solar irradiance, layer thickness, and so on.

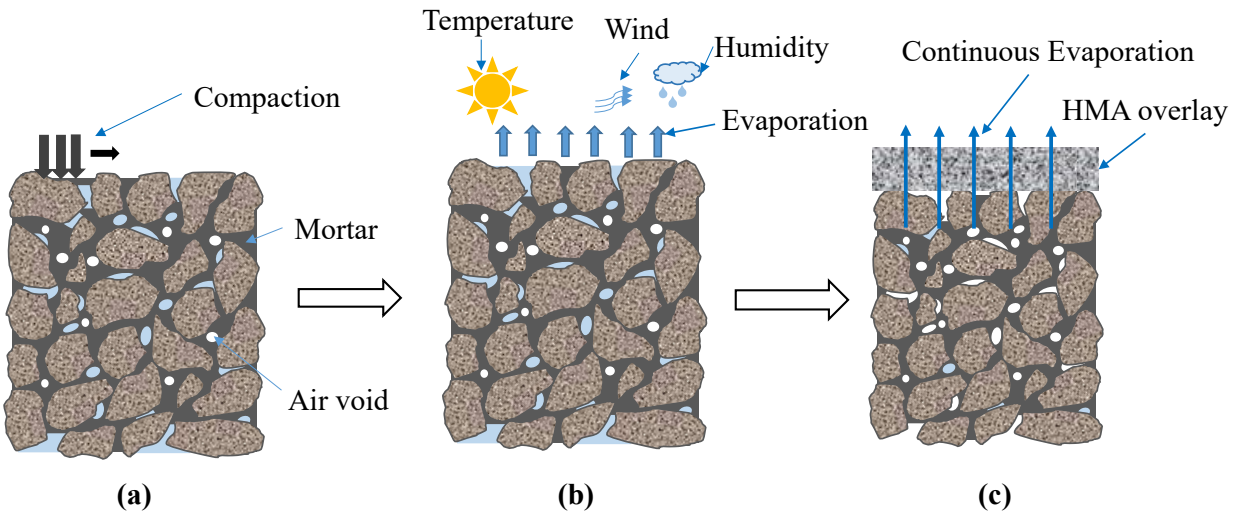

Fig. 1. Moisture migration in BE-CIR pavement: (a) initial full-depth CR mixture after the compaction stage; (b) evaporation during the curing stage; (c) continuous evaporation during the in-service stage.

Many pieces of research have been done to characterize the drying behavior of the BE-CIR mixture. Evaporation dynamics of the BE-CIR curing process were investigated by evaporation tests and hydraulic conductivity tests, using water loss and evaporation rate as indicators (Saadoon et al., 2017). Based on this, an evaporation depth prediction model was proposed and related to the mechanical properties. In-situ tests were conducted to investigate the moisture behavior inside the pavement structure. Ground-penetrating radar, nuclear density and moisture gauge, time-domain reflectometer, and capacitance moisture sensors were used to monitor and predict the evolution of the water content inside the BE-CIR pavement (Kim et al., 2011; Ogbo et al., 2022; Zhao et al., 2022). The study of water vapor movement inside the mixture primarily aims at hot-mix asphalt pavement and its moisture damage resistance. Based on Fick's first law, researchers developed simple devices to measure the effective diffusion coefficient of mixtures, a material property affecting the moisture diffusion behavior (Arambula et al., 2010). Devices based on Fick's second law and thermocouple psychrometers can also measure the effective diffusion coefficient of mixtures, but the method is complicated (Apeagyei et al., 2014). It is worth noting that the aforementioned drying behavior studies were conducted under specific constant environments, and the humidity inside the pavement was assumed to be uniformly distributed. Although some patterns have been derived from the existing studies, theoretical analyses based on heat and mass transfer are still lacking, making it difficult to explicate the BE-CIR drying behavior in a field pavement curing environment with real-time variations in temperature and RH. In addition, the overlay placement timing of BE-CIR pavement after compaction in construction mainly relies on experience and lacks theoretical guidance for different curing environments the contractors may encounter in practice.

To fill this gap, the primary objectives of this research are to 1) establish a drying behavior model of BE-CIR pavement under the effect of the moisture-heat coupling before overlay placement; 2) predict moisture equilibrium timing under natural curing environments based on the model.

2 METHODS

2.1 Governing Equations

The drying behavior of BE-CIR pavement is a result of combined mass and heat transfer, and the energy and continuity equations govern the migration of heat and moisture. Ambient temperature and RH are critical factors affecting the drying behavior. To model the drying behavior inside the BE-CIR pavement, following assumptions were taken based on the properties of the curing phase of BE-CIR

pavement: (1) ignoring capillary; (2) ignoring liquid water convection; (3) no chemical reactions; (4) constant geometry.

2.1.1 Heat Transfer

Heat transfer includes three components: heat conduction, heat convection, and heat radiation (Sun and Sheng, 2020). Heat conduction inside the mixture was calculated using the energy conservation equation, as shown in Eq. (1) (M. L. Hoang et al., 2003).

$$\left(\rho C_p\right)_{eff}\frac{\partial T}{\partial t}-\nabla\cdot\left(k_{eff}\nabla T+L_{\mathrm{v}}\delta_p\nabla(\varphi p_{\mathrm{sat}})\right)=Q \quad (1)$$

Where $\left(\rho C_p\right)_{eff}$ = effective volumetric heat capacity at constant pressure; T = temperature; k_{eff} = effective thermal conductivity; L_{v} = latent heat of evaporation; δ_p = vapor permeability; φ = relative humidity; p_{sat} = vapor saturation pressure; Q = heat source.

Heat flux at the pavement surface was calculated by Newton's cooling equation shown in Eq. (2) (Winterton, 1999). Heat transfer coefficient was obtained based on ambient wind speed and width of the pavement surface.

$$Q_c=h(T_{\mathrm{amb}}-T)\ =\ \frac{Nu\times\beta}{L}(T_{\mathrm{amb}}-T) \quad (2)$$

Where Q_c = heat flux by convection; h = heat transfer coefficient; T_{amb} = ambient temperature; Nu = Nusselt number; β = air thermal conductivity; L = characteristic length.

Radiative heat transfer included radiation from the environment to the pavement and from the pavement to the environment. The radiation from the pavement to the environment is calculated by the Stephan-Boltzmann law shown in Eq. (3) (Nuijten and Høyland, 2017).

$$Q_F=\varepsilon\sigma\left(T^4-{T_{\mathrm{amb}}}^4\right) \quad (3)$$

Where Q_F = effective radiation rate; ε = surface emissivity; σ = Stefan-Boltzmann constant.

2.1.2 Moisture Migration

Moisture migration in the BE-CIR pavement structure consists of diffusion only. According to the continuity equation and the assumptions mentioned above, Eq. (4) demonstrates governing equation for moisture (Welty et al., 1976).

$$\xi\frac{\partial\varphi}{\partial t}+\nabla\cdot g_w=G \quad (4)$$

$$\xi=\frac{\partial w(\varphi)}{\partial\varphi} \quad (5)$$

Where ξ = moisture storage capacity; g_w = diffusive flux for vapor; G = moisture source; w(φ) = water content.

Fick's law was employed to describe the moisture flux. The effective diffusion coefficient expressed in terms of concentration was rewritten as the vapor permeability expressed in terms of pressure, as shown in Eq. (6) (Paul et al., 2014).

$$g_w=-\rho_{\mathrm{g}}D_{eff}\nabla\omega_{\mathrm{v}}=-\frac{M_{\mathrm{v}}D_{eff}}{R_{H_2O}}\frac{M_{\mathrm{a}}}{(x_{\mathrm{a}}M_{\mathrm{a}}+x_{\mathrm{v}}M_{\mathrm{v}})^2}\nabla p_{\mathrm{v}}=-\delta_p\nabla(\varphi p_{\mathrm{sat}}) \quad (6)$$

Where ρ_g = vapor density; D_{eff} = effective diffusion coefficient of BE-CIR mixture; ω_v = vapor mass fraction; M_v = molar mass of water vapor; M_a = molar mass of dry air; R_{H_2O} = universal gas constant of water vapor; p_v = water vapor partial pressure.

Wide variations in the temperature of the pavement structure can significantly affect the magnitude of vapor permeability, so the Arrhenius equation was adopted, which proved to be suitable for expressing temperature-dependent reaction rates (Ma et al., 2022).

$$D_{eff} = Ae^{-\frac{E_a}{R_{H_2O}T}} \quad (7)$$

Where A = preexponential factor; E_a = activation energy.

2.2 Experimental Study

Field and laboratory measurements were implemented to clarify the drying behavior of BE-CIR pavement after compaction and obtain the physical parameters of materials.

2.2.1 Field Monitoring for BE-CIR Pavement

Field monitoring for the BE-CIR pavement after compaction was executed in a pavement maintenance project at Fenguan Highway (G15) in Lianyungang, Jiangsu Province of China. A trial section with a total length of more than 4 km was treated by the BE-CIR technology, which recycled the original top and middle layer into the BE-CIR layer. During construction, 3.3% cationic slow-setting emulsified asphalt, 2.2% Ordinary Portland Cement (P.O 42.5), 2.8% extra water, and 100% old pavement were recycled into the new BE-CIR layer. Gradation of the BE-CIR layer is shown in Fig. 2, and the properties of the emulsified asphalt are presented in Table 1. The maximum dry density method (MOT, 2019), Marshall Stability Test, and Indirect Tensile Strength Test were employed to determine the optimum moisture content and the optimum bitumen emulsion content. After recycling, the BE-CIR layer must be cured for a period before the overlay is placed. Sensors were buried at road pile number K795+500, located in the construction section from K794+636 to K796+372, with a total length of 1.736 km. Four different depths were chosen to embed sensors to record the gradient variation characteristics of temperature and humidity in the BE-CIR layer. The recording lasted 163 hours, from the recycle completion to the overlay placement. Depths 1 to 4 corresponded to 5, 35, 65, and 95 mm from the BE-CIR layer upper surface and were denoted as D1, D2, D3, and D4. Two humidity sensors and one temperature sensor were buried at each depth. The humidity sensor measured the moisture condition of solid using the Frequency Domain Reflectance method, and the output was defined as the humidity index (HI), which varied between 0 and 1. Laboratory tests were implemented to obtain the relationship between water content and HI. A functional equation between RH and water content was determined as well. Based on this, the relationship between HI and RH was obtained. Considering the influence of the curing environment on moisture and temperature distribution inside the BE-CIR layer, ambient temperature, RH, wind speed, and solar radiation during the monitoring were collected from local weather stations. More specific information can be found in the authors' previous study (Zhao et al., 2022).

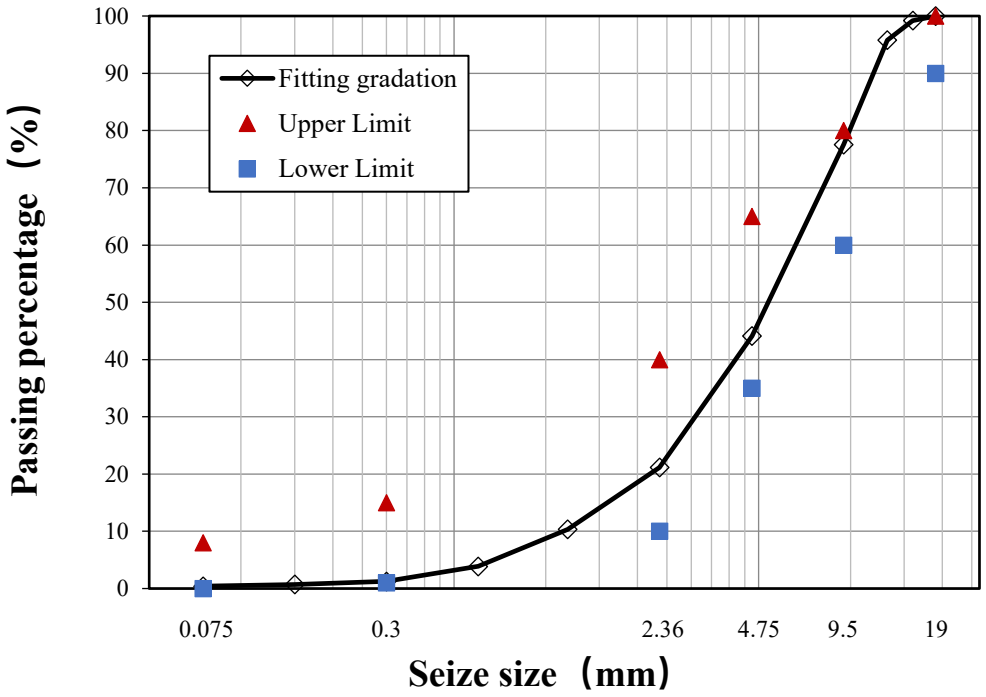

Fig. 2. Aggregate gradation of BE-CIR mixture.

Table 1
Properties of emulsified bitumen.

Properties	Value
Residual content (%)	63.8
Penetration (25 °C; 0.1 mm)	62.1
Softening point (°C)	50.6
Ductility (15 °C; cm)	110
Sieve residue (1.18 mm; %)	0.03
Storage stability (5 d, 25 °C; %)	0.18
Storage stability (1 d, 25 °C; %)	0.06

2.2.2 Indoor monitoring for BE-CIR mixture

Considering the inconvenience of modeling due to the complex field conditions, laboratory mixture tests were implemented as well. 150 mm diameter and 100 mm high mixture specimens were prepared by 30 times gyratory compaction. The RAP was sourced entirely from the trial section field, the gradation was not adjusted, and the material composition was designed to be the same as in the field. A special curing procedure was adopted to simulate the drying behavior in the field condition. Waterproofing membranes were covered on the bottom and sides of the mixtures to achieve unidirectional evaporation (Zhao et al., 2023). The mixtures were cured at a constant temperature and humidity chamber for 28 days at 45% RH, with curing temperatures at 25°C, 30°C, 35°C, 40°C, and 45°C, respectively. On day 1, 3, 7, 14, and 28, the mixtures were taken out and measured for mass, which were combined with the initial mass to calculate water loss. Michaelis-Menten model is commonly used to describe the tendency of material properties to increase rapidly over time and then stabilize, as in Eq. (8) (Graziani et al., 2018). Hence, this model was used to define the relationship between curing time and water loss.

$$y(t) = \frac{y_A \cdot t}{h_y + t} \quad (8)$$

Where $y(t)$ = water loss; y_A, h_y = fitting parameters with physical meaning, y_A is stabilized value, and h_y is the required curing time to reach half of the stabilized value.

Another fully cured mixture slice was prepared, and the effective diffusion coefficient was tested at different temperatures according to ASTM E96 (ASTM, 2014). The effective diffusion coefficient was converted to vapor permeability according to Eq. (6).

Due to the difficulty of embedding sensors in the mixture specimens to obtain variations of internal moisture distribution, X-ray computed tomography (X-CT) was implemented. Two mixture specimens 100 mm in diameter and 100 mm in height were prepared with the same material composition as the abovementioned mixture. The curing temperature of these two specimens was 25°C and 40°C. Specimens were scanned on day 0, 3, and 7 after compaction. Scan parameters were set as voltage 240 kV and scanning current 0.72 mA. Body pixels of images were set to 60.1 μm with 1747*1747 pixels per slice. Noise reduction and grayscale transformation were implemented to obtain clearer images. The voids at different moments were extracted by the OTSU method and reconstructed. Scanned images of different curing days were rotated and panned for alignment adjustment. Define the earlier scanned image as the base image and the later scanned image as the processed image. Boolean operations were performed on the processed image and the base image. The portions that were void in the base image and non-void in the processed image were extracted. This portion represented the void change during the curing time, which was the location of dispersed water. The value obtained by dividing the portion's area by the slice's area was defined as the water loss C_{wl}. More specific information can be found in the authors' previous study (Jiang et al., 2023).

2.3 Model Establishment

2.3.1 Laboratory Mixture Model

According to the laboratory mixture test's specimen dimension and curing conditions, a numerical model was established, as shown in Fig. 3(a).

Material parameters: Heat and mass transfer parameters of the BE-CIR mixture, including thermal conductivity, heat capacity at constant pressure, vapor permeability, and moisture storage function, were determined from laboratory tests.

Boundary conditions: The bottom and sides of the model were moisture and heat insulated, with only the upper surface allowing exchange of moisture and heat flux with the environment.

Initial conditions: Initial HI of the whole model was set to be 0.75 according to the initial water content of the mixture, and the initial temperature was set to be 35°C.

Environmental conditions: The ambient RH was kept at 30% consistently, while the ambient temperatures were set to 25°C, 30°C, 35°C, 40°C, and 45°C, respectively.

Calculation settings: The simulation duration was 28 days; the step size was varied over time to improve the stability and efficiency of the simulation.

Observation points were assigned at 10mm intervals at the cylinder center, except for the upper and lower surfaces, with nine observation points employed for data analysis.

2.3.2 Field Pavement Model

As shown in Fig. 3(b), a model consistent with the field pavement structure was built. The model was 10.76m in depth with five structural layers. The overlay was not built up as it only simulated the situation before it overlaid. The length and width were 3.75m, which means one lane width. In order to ensure simulation accuracy, temperature variations were calculated for each structural layer. Due to the insensitivity of the remaining layers to moisture and computational efficiency, only the moisture distribution inside the BE-CIR layer was simulated.

Material parameters: The heat and mass transfer parameters for the BE-CIR layer were identical to those used in the laboratory mixture model. Material parameters for the remaining structural layers were collected from literature.

Boundary conditions: For the temperature simulation, corresponding to the constant temperature layer in geography, the temperature at the bottom of the subgrade was constant at 15°C. The sides of the model were thermally insulated. Heat exchange with the environment existed at the model's upper surface. For the moisture simulation, the bottom and sides of the BE-CIR layer were set as moisture insulation. Moisture exchange with the environment existed at the model's upper surface.

Initial conditions: Initial HI and temperature at each depth of the BE-CIR layer were obtained from field-measured data.

Environmental conditions: The ambient temperature, RH, wind speed, solar irradiance, and other data were collected from the weather station where the field section is located.

Calculation settings: The simulation duration was seven days. Starting time was 16:00 on May 23, 2021, corresponding to the sensors' burial time. The maximum solution step was 1 hour to ensure simulation accuracy.

Corresponding to the burial depths of the sensors, four observation points were assigned to monitor temperature and moisture variations inside the BE-CIR layer.

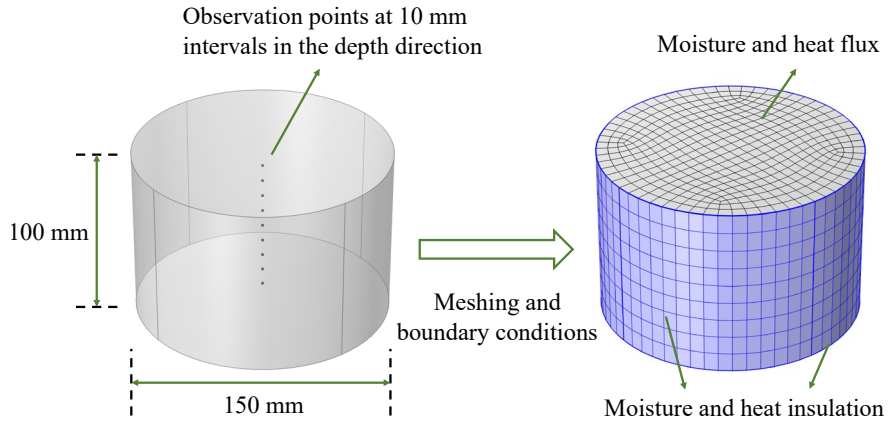

(a) Laboratory mixture model schematic

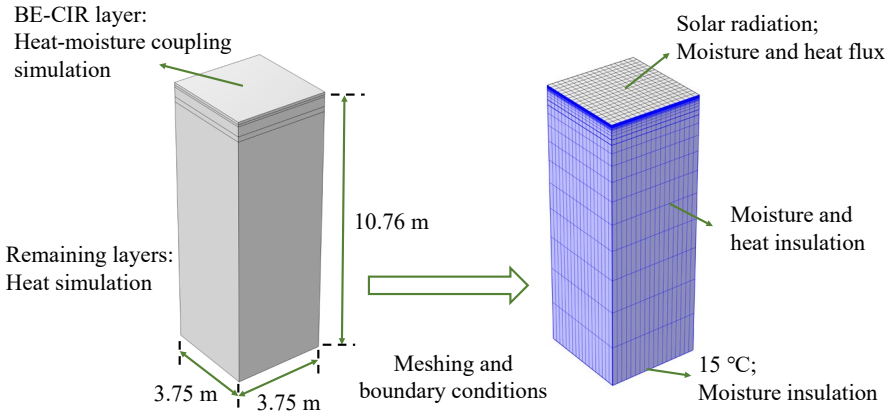

(b) Field pavement model schematic

Fig. 3. Numerical simulation model.

3 RESULTS AND DISCUSSION

3.1 Drying Behavior Model

Based on Fick's first law, the effective diffusion coefficients were tested at different temperatures, as shown in Fig. 4. The Arrhenius equation was used to fit the effective diffusion coefficient to temperature as in Eq. (9).

$$D_{eff} = 89.8 \times e^{-\frac{14426}{8.314T}} \quad (9)$$

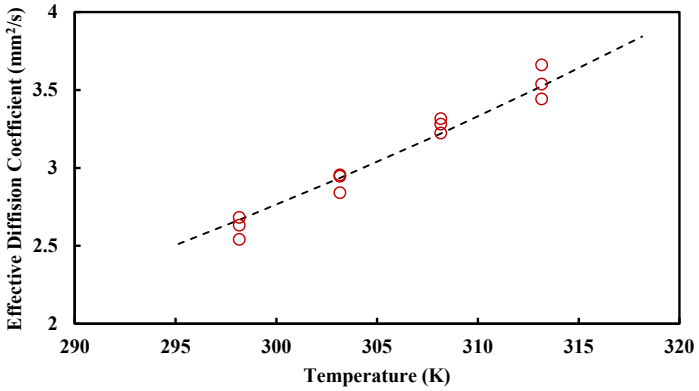

Fig. 4. Fitting model for the effective diffusion coefficient and temperature.

Fig. 5 shows the X-CT test results. On the third day, the BE-CIR mixtures with different curing temperatures had no significant gradient characteristics in the depth direction. On the seventh day, the moisture gradient characteristics exhibited in the upper 90 mm for the curing temperature of 40°C and in the upper 45 mm for the curing temperature of 25°C.

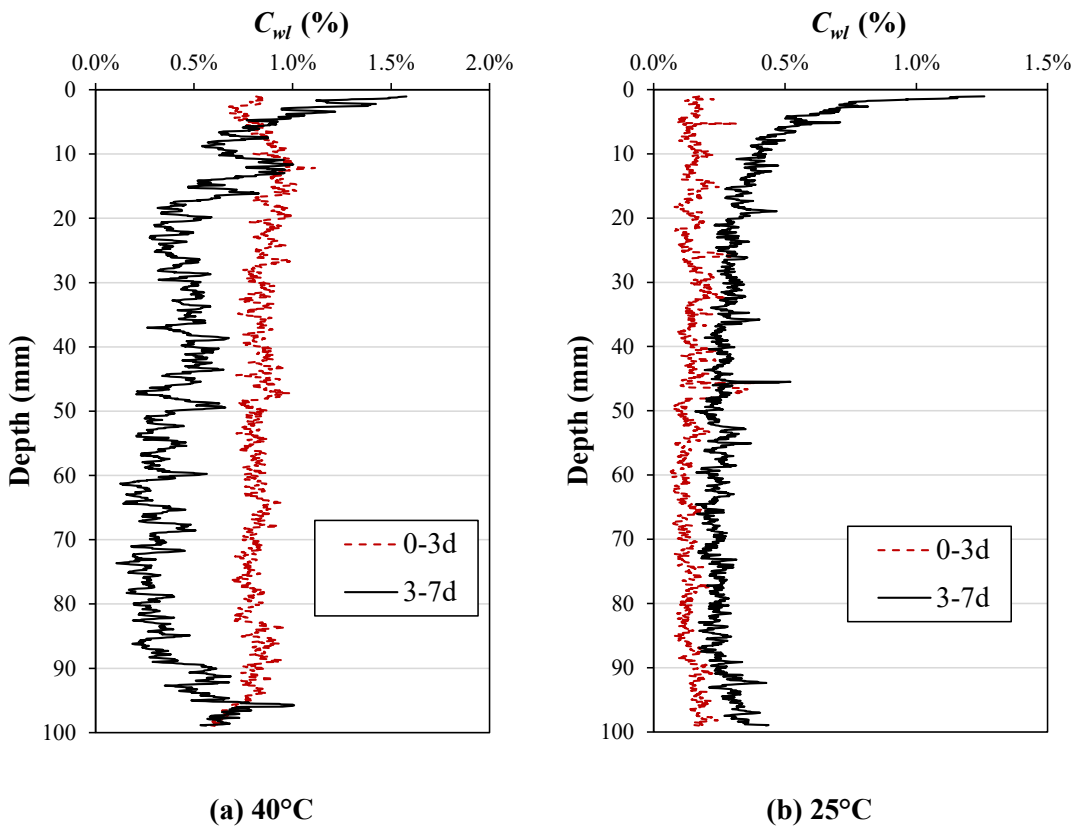

(a) 40°C **(b) 25°C**

Fig. 5. Variation of C_{wl} in depth.(Jiang et al., 2023)

3.1.1 Time-variable Coefficient Calibration

The laboratory mixture model was calculated, and the result is shown in Fig. 6. In the first seven days, the measured water loss increased rapidly while the simulated water loss grew slowly, and the difference between the simulated and measured values was more evident with higher curing temperatures. After the seventh day, the difference between the measured and simulated values were gradually stabilized. It indicated that the effective diffusion coefficient used in the simulation was smaller than the actual value at the beginning of curing. This phenomenon could be attributed to the different strength formation mechanisms of BE-CIR and hot-mix asphalt mixture. At the early stage of curing, non-organic additives such as cement in the BE-CIR mixture had not formed a dense mesh structure, asphalt droplets were dispersed in the emulsion, and the channel for moisture diffusion was unrestricted, so moisture evaporated fast. With the increasing curing time, the non-organic additives were gradually hydrated. At the same time, the asphalt droplets aggregated to form the film. The channels for moisture diffusion were gradually blocked, which decreased the effective diffusion coefficient with the curing time. According to the analysis, the effective diffusion coefficient obtained from the laboratory tests was a physical property of the BE-CIR mixture that had already developed strength, which was much smaller than that in the early curing stage. Therefore, it is necessary to introduce a time-variable coefficient to correct the effective diffusion coefficient to reflect the time-dependence of the effective diffusion coefficient of the BE-CIR mixture (Apeagyei et al., 2015).

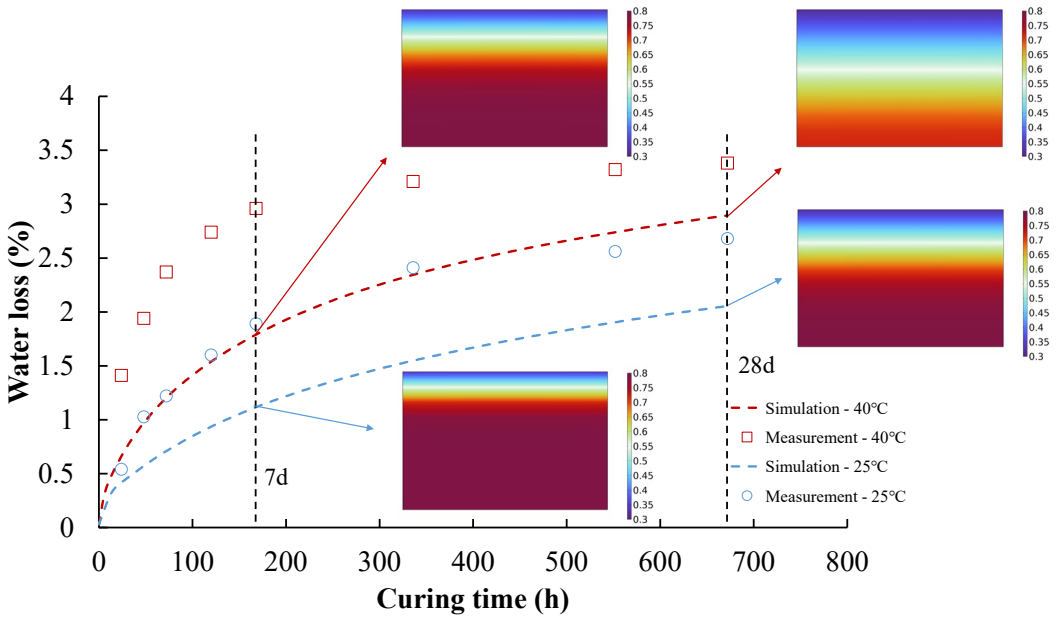

Fig. 6. Simulation results of model uncorrected by the time-variable coefficient.

A time-variable effective diffusion coefficient relationship was constructed to clarify the decay pattern of the effective diffusion coefficient during the curing process. It has been demonstrated that the effective diffusion coefficient exhibited a tendency to decrease with increasing modulus in the asphalt mixture. For the BE-CIR mixture, the relationship between strength and residual water content during the curing process could be described by a linear function (Graziani et al., 2018). The residual water content was defined as the water content of the mixture at the initial moment minus water loss at the current moment, while the relationship between water loss and the curing time can be described by the Michaelis-Menten model (Graziani et al., 2018). Based on the relationship between the curing time, water loss, residual water content, strength, and effective diffusion coefficient, Eq. (10) defined an expression for the time-variable coefficient $\varphi(t)$. When $t = 0$, $\varphi(t) = e^{ky_A}$, and when $t = +\infty$, $\varphi(t) = 1$, which corresponds to the return of $\varphi(t)$ to the measured effective diffusion coefficient after a period of curing.

According to the laboratory tests results, y_A and h_y were temperature dependent and could be fitted by linear and exponential functions, respectively, as in Eq. (11) and Eq. (12).

$$\varphi(t) = e^{k\left(y_A - \frac{y_A \cdot t}{h_y + t}\right)} \quad (10)$$

$$y_A = 0.0268T + 2.428 \quad (11)$$

$$h_y = 27.007e^{-0.072T} \quad (12)$$

Where k = adjustment coefficient to correct the effective diffusion coefficient at the initial moment of curing.

The adjustment coefficient was set to 1. The calculation results of the modified model with the time-variable coefficient are shown in Fig. 7. The relationship curves between water loss and curing time changed significantly after introducing the time-variable coefficient. The simulated results, closer to the measured values, indicated that adopting the time-variable coefficient was effective.

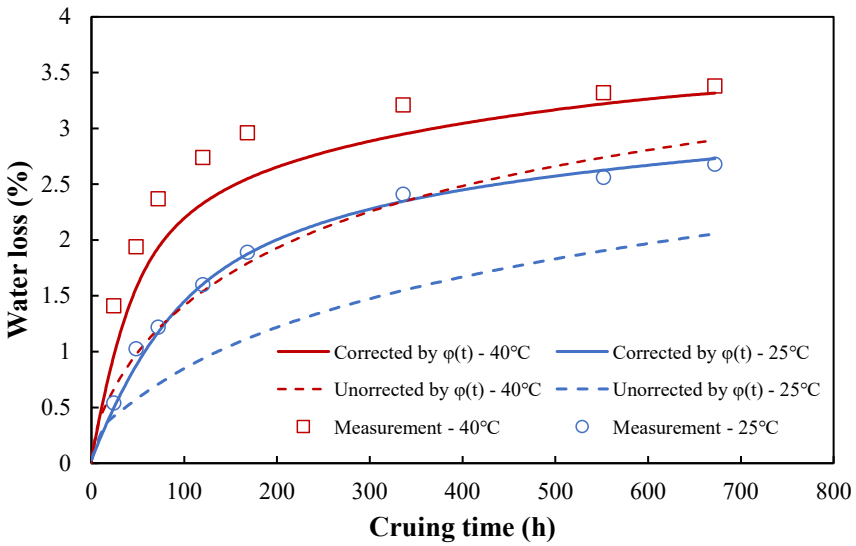

Fig. 7. Comparison of simulation results after introducing the time-variable coefficient.

3.1.2 Depth Correction Coefficient Calibration

Fig. 8 shows the humidity distribution inside the mixture in depth on the third day and the seventh day of curing. On the third day of curing, significant gradient characteristics were present between 0-50 mm depth for both mixtures at two curing temperatures. On the seventh day of curing, the mixture cured at 40°C demonstrated a moisture gradient over almost the entire depth, whereas the mixture cured at 25°C was characterized by a moisture gradient only between 0-60 mm at depth. By comparing Fig. 5 and Fig. 6, the simulated and measured values showed different patterns in depth, which was attributed to the same effective diffusion coefficient of the model over the depth. With the BE-CIR material losing moisture, the combined effect of bitumen emulsion breaking and cement hydration formed the material's strength while at the same time blocking the channels for moisture diffusion and decreasing the effective diffusion coefficient. Measured and simulated results demonstrated that the moisture evaporated from the upper surface of the mixture and gradually dried the whole mixture downward along the depth direction. This indicated that the top-to-bottom moisture drying process of the material during the actual curing process resulted in a similar top-to-bottom gradient in the effective diffusion coefficient of the material. A drier depth position implied a lower effective diffusion coefficient. A depth correction coefficient ω was proposed to characterize this phenomenon. This coefficient was affected by φ, with high φ leading to high effective diffusion coefficient. Meanwhile, the strength formation was an irreversible process, and the strength would not vary remarkably in a short time due to variations in φ. Consequently, the depth correction coefficient ω should decrease gradually with increasing curing time and eventually to 1. In summary, the depth correction coefficient should be expressed as a function affected by φ and time t, denoted as $\omega(\varphi, t)$. The depth correction coefficient was essentially a time-variable coefficient in depth, so the same exponential relationship was employed to describe the depth correction coefficient, as shown in Eq. (13).

$$\omega(\varphi, t) = e^{\left(\frac{\varphi}{t+m}\right)} \tag{13}$$

Where m = adjustment coefficient that controls the timing of the depth correction coefficient taking effect. m can be preset to 0.01 to ensure $\omega(\varphi, t)$ makes sense at t = 0.

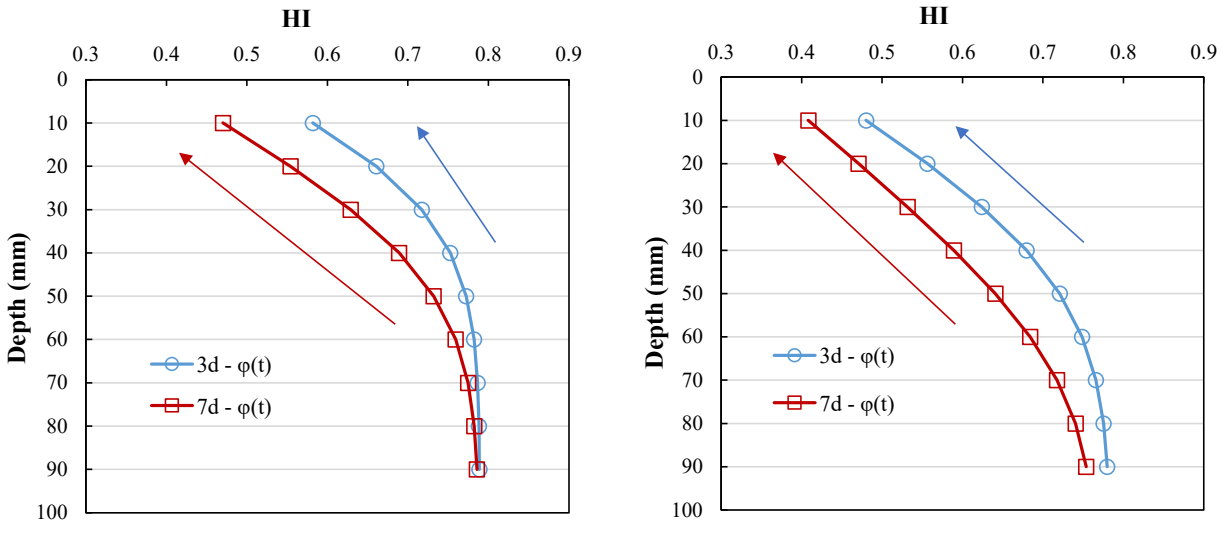

(a) 25°C **(b) 40°C**

Fig. 8. Moisture distribution in depth.

The model modified by the time-variable coefficient and depth correction coefficient was calculated, and m was finally determined to be 0.6. Calculation results are shown in Fig. 9. The results indicated that the difference in moisture distribution at each depth was reduced and close to the measured results.

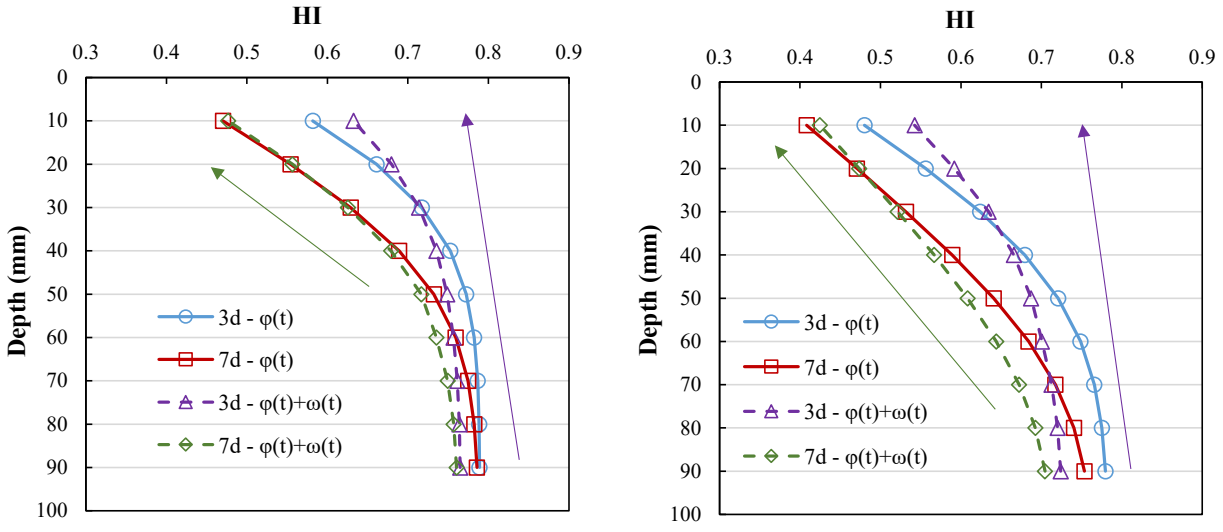

(a) 25°C (b) 40°C

Fig. 9. Effect of depth correction coefficient on the moisture distribution in depth.

The final form of the effective diffusion coefficient after modification by the time-variable coefficient and depth correction coefficient is shown in Eq. (14) and Eq. (15). In order to verify the

accuracy of the model after the modification of two coefficients, the model was employed to calculate the water loss of the mixture at curing temperatures of 25°C, 30°C, 35°C, 40°C, and 45°C, respectively. coefficient of determination (R^2, Eq. (16)) and Root Mean Square Error (RMSE, Eq. (17)) were adopted to evaluate the simulation results. Fig. 10 demonstrates the comparison results between simulated and measured values for different curing days and different curing temperature. The results showed that all points were close to the line of equality, and the R^2 reached 0.956, meaning that the simulation was accurate.

$$D_{eff} = Ae^{-\frac{E_a}{R_{H_2O}T}} \cdot \varphi(t,T) \cdot \omega(\phi_w,t) \quad (14)$$

$$D_{eff} = 89.8e^{-\frac{1735}{T}} \times e^{\left(0.0268T+2.428-\frac{(0.0268T+2.428)\cdot t}{27.007e^{-0.072T}+t}+\frac{\varphi}{t+0.6}\right)} \quad (15)$$

$$R^2 = 1 - \frac{\sum_{i=1}^{m}(\hat{y}_i - y_i)^2}{\sum_{i=1}^{m}(y_i - \bar{y})^2} \quad (16)$$

$$RMSE = \sqrt{\frac{1}{m}\sum_{i=1}^{m}(y_i - \hat{y}_i)^2} \quad (17)$$

Where $\hat{y}_i$ = simiulated value; y_i = measured value; $\overline{y_i}$ = mean of the measured value.

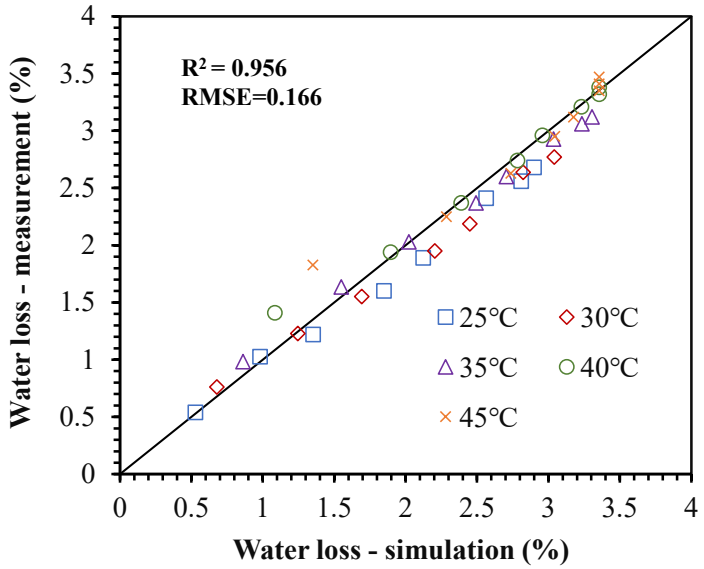

Fig. 10. Evaluation of model corrected by two coefficients.

3.1.3 Model Validation

The two correction coefficients obtained from the laboratory mixture model were applied to the field pavement model calculations to validate the accuracy of the model parameters.

Fig. 11 illustrates the results of temperature field simulation for the BE-CIR layer. Fig. 12 compares the simulated and measured results of the temperature field. The comparison results showed that the simulated the R^2 reached 0.93 and the RMSE was only 1.655 °C. The model could accurately simulate pavement temperature changes.

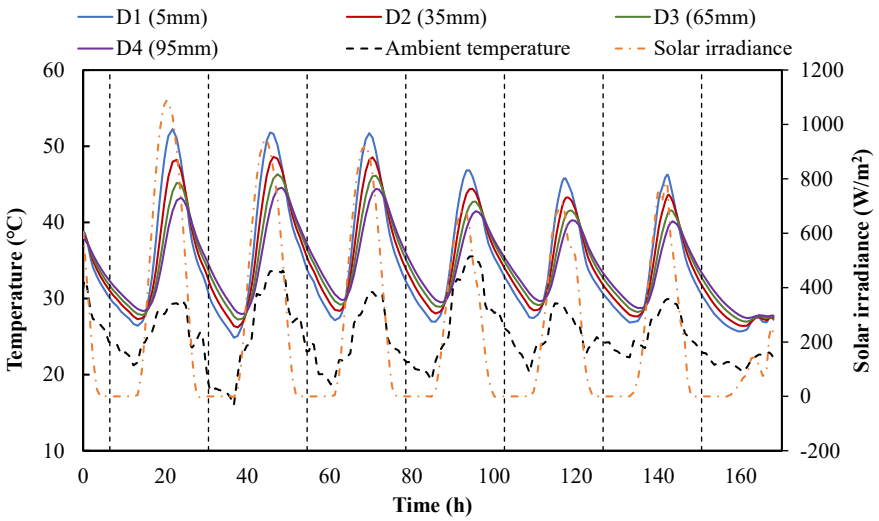

Fig. 11. Simulation result of temperature field.

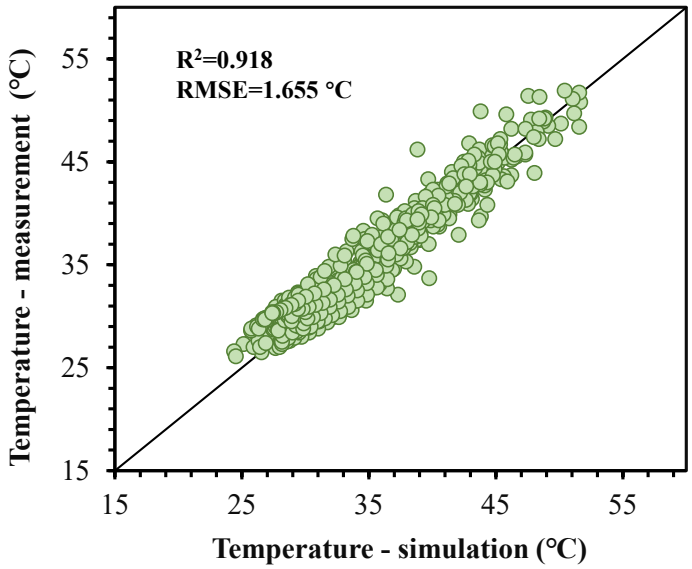

Fig. 12. Evaluation of temperature field simulation results.

Fig. 13 illustrates the HI simulation results for the BE-CIR layer. Unlike the uniform initial humidity distribution of the laboratory mixture model, a humidity gradient distribution had been characterized inside the pavement after compaction. There were different degrees of delay in humidity decline at each depth. After about 30 hours of humidity decrease, the moisture movement inside the BE-CIR layer stabilized and only slightly fluctuated with ambient RH variation. The simulated results showed a consistent trend with the measured results.

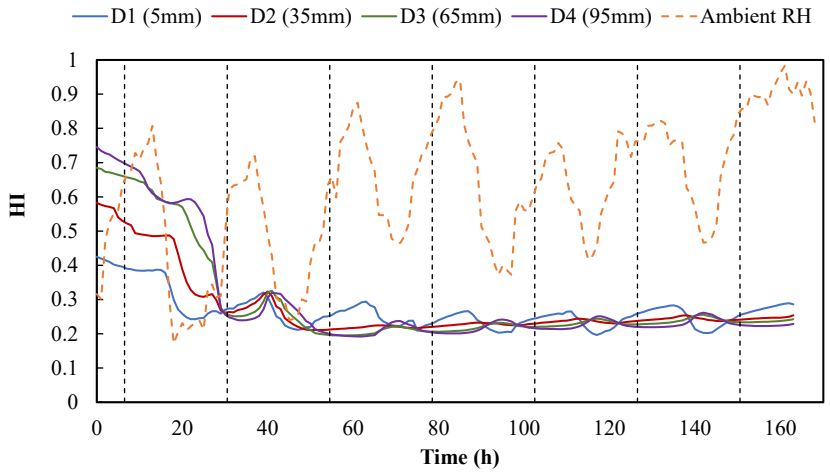

Fig. 13. Simulation results of HI at each depth.

Fig. 14 demonstrates the simulated values of HI at each depth compared to the measured values. The corrected and uncorrected models were computed separately to validate the two correction coefficients. For the uncorrected model, the HI of D2 and D3 were constantly higher than the measured values, and the HI of D4 was also higher than the measured values after the 11th hour. This phenomenon indicated that the effective diffusion coefficient uncorrected by the time-variable coefficient was too small in the early curing stage. This resulted in a slow moisture diffusion inside the pavement and moisture accumulation. The large fluctuations in HI at D1 indicated that the effective diffusion coefficient uncorrected by the depth correction coefficient was large at that depth, making HI susceptible to ambient RH. The computational results of the uncorrected model verified the necessity of correcting the effective diffusion coefficients for time and depth. The calculated results of the corrected model fitted the measured data better than those of the uncorrected model, but there were still gaps. The decrease rate of HI was faster for the measured values. On the one hand, this might be related to the complex curing conditions of the actual pavement, where pavement compaction by vehicles after recycling might result in accelerated moisture migration. On the other hand, both sides and bottom of the field pavement model were set to be moisture insulated, whereas they were permeable to moisture in the actual pavement curing environment, which led to a rapid drop in humidity.

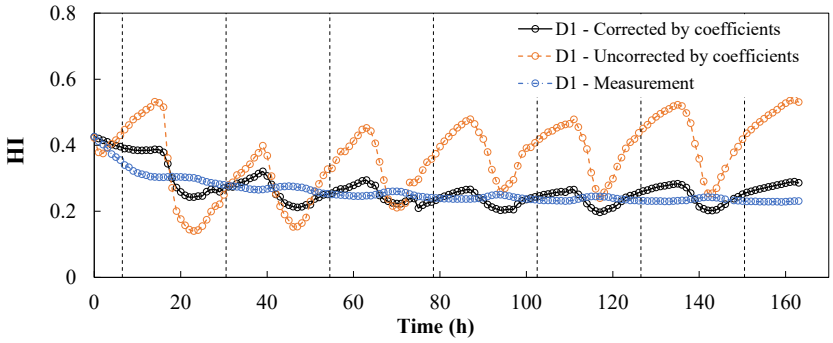

(a) Depth1 - 5mm

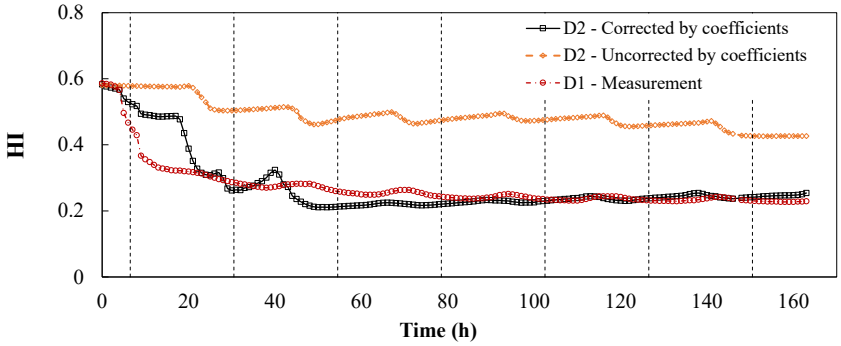

(b) Depth2 - 35mm

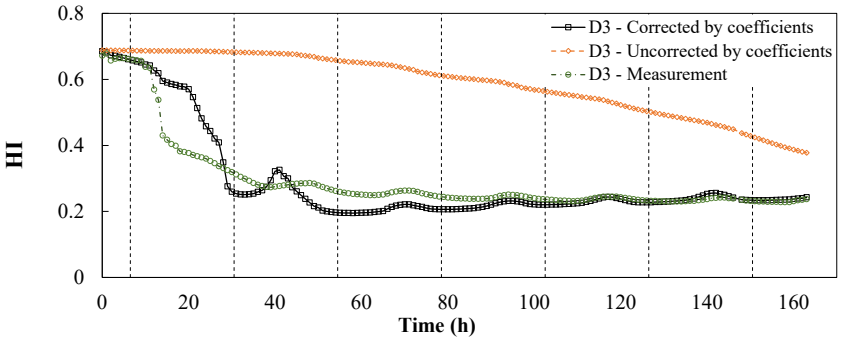

(c) Depth3 - 65mm

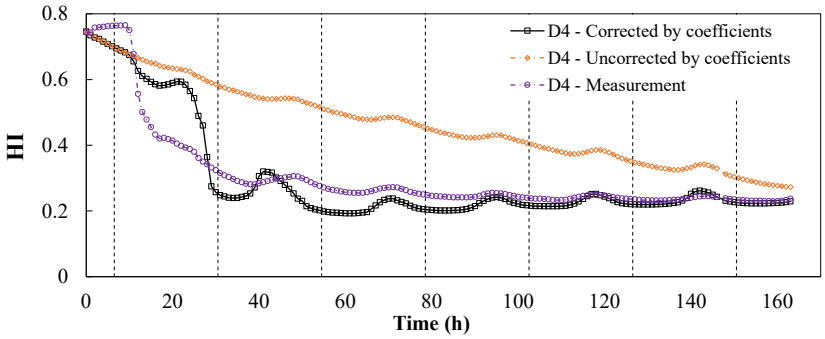

(d) Depth4 - 95mm

Fig. 14. Humidity comparison between simulation and measurement at each depth.

Fig. 15 evaluated the difference between the calculated results of the corrected and uncorrected models and the measured values, respectively. The results suggested that the difference between the calculated results of the uncorrected model and the measured values was significant, with the R^2 less than 0. Most of the simulated values were significantly greater than the measured values. The calculated results of the corrected model were closer to the measured values, with the R^2 up to 0.747 and the RMSE was only 0.05. The comparison indicated that the correction of the two coefficients can greatly improve the accuracy of humidity field simulation results.

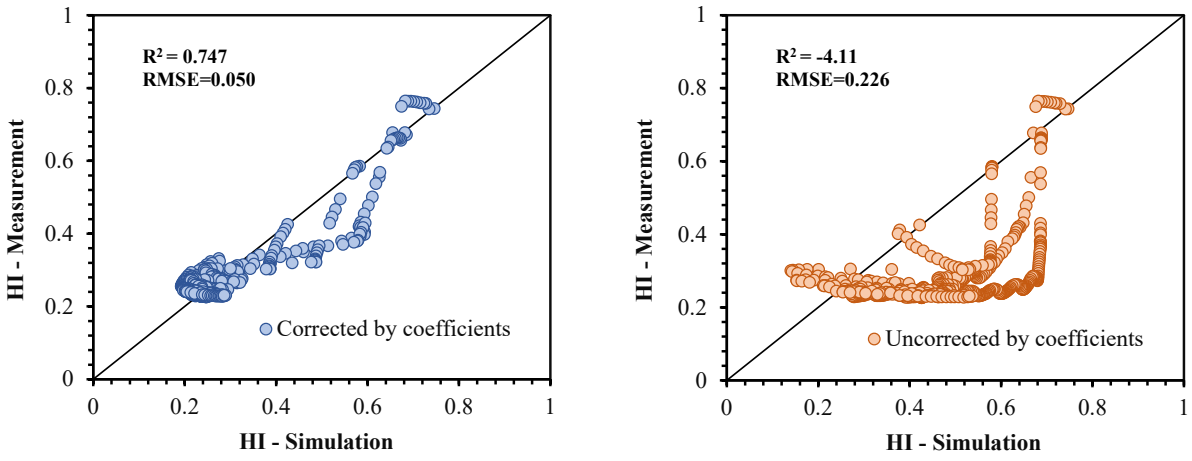

(a) Corrected by coefficients (b) Uncorrected by coefficients

Fig. 15. Evaluation of simulation results.

By combining with the temperature field simulation results, it was observed that the model corrected by the two coefficients could accurately simulate and predict the temperature field and humidity field under a natural pavement curing environment. The validity of the drying behavior model was verified.

3.2 Effect of Curing Environment on Drying Behavior

The duration between compaction and overlay placement on BE-CIR pavement significantly impacts construction economics. Early overlay placement and traffic opening reduce the impact of construction on community transportation capacity. The moisture distribution inside the BE-CIR pavement is an important factor influencing the timing of overlay placement. Generally, a higher moisture evaporation degree corresponds to a stronger pavement strength. Nevertheless, due to the difficulty of real-time monitoring of the moisture inside pavement, constructors often determine the overlay placement timing through coring tests and empirical judgment, which raises the economic expense to some extent and is detrimental to long-term healthy pavement service. The drying behavior prediction model based on two correction coefficients can calculate the moisture distribution of the BE-CIR layer under different natural curing environments in real-time, which is vital to guide the placement timing of the overlay.

Two typical working conditions were selected to clarify the effect of the curing environment on the drying behavior of BE-CIR pavement. The different working conditions were distinguished based on temperature and RH, which were categorized into three classes, i.e., low, medium, and high. The grade thresholds for temperature were 17°C and 25°C, and for RH were 55% and 90%. Condition 1 was rainy summer days with medium temperature and high humidity, and condition 2 was regular fall days with low temperature and medium humidity. Meteorological data of Lianyungang, Jiangsu Province, China, where the trial section is located, from 2021/7/27 16:00 to 2021/8/3 16:00 and from 2021/10/10 16:00 to 2021/10/17 16:00 were collected to serve as curing environments for the two conditions. As a comparison, the curing environment for the trial section was dry summer days with high temperature and low humidity. These three conditions represented the relatively extreme environments encountered during construction. The cure duration required for moisture equilibrium for the remaining six conditions was almost exclusively between these three conditions. Fig. 16 illustrates the ambient temperature and RH of these three curing environments. The measured humidity distribution used for model validation was employed as the initial value for this simulation, and the temperature distribution at the initial moment was set to be the same as the ambient temperature. The remaining simulation settings were consistent with those of the field pavement model.

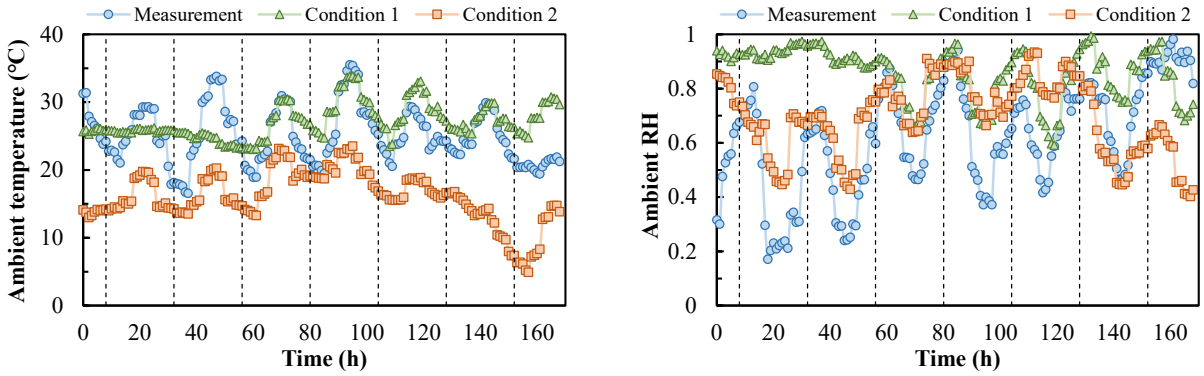

(a) Ambient temperature (b) Ambient RH

Fig. 16. Ambient temperature and RH for different working conditions.

Fig. 17 shows the HI calculation result of the BE-CIR layer for condition 1. It could be observed that the moisture variation inside the BE-CIR layer was in three stages. In the first stage, the HI remains constant at all depths. Corresponding to the summer rainy days, the ambient RH was higher than 0.9 for the first 38 hours of this condition, while the ambient temperature was kept around 25°C. The HI at each depth increased slowly with time during the first 38 hours and generally remained at a high level. In the second stage, the HI decline at all depths decreased in the order of depth. After the 38th hour, rainfall weakened, and ambient RH fluctuated periodically. Between the 38th and 120th hour, the HI at all depths showed an overall decreasing trend with increasing time, which was attributed to the declining ambient RH and increasing temperature, implying the evaporation of moisture inside the pavement. In the third stage, the HI decline ended and remained stable. After the 120th hour, the HI fluctuated around 0.26 at all depths. Although ambient RH remained at a high level, benefiting from the correction of the time-variable and depth correction coefficients, the fluctuation of HI was slight. According to the trial section's test results, HI dropping to 0.3 meant a general end of drying and overlay placement. For condition 1, which represented a hot rainy day, 120 curing hours were required for moisture evaporation, implying up to the standard of overlay placement. From the 40th to the 120th hour at the end of the rainfall, it took 80 hours for the BE-CIR layer to reach a moisture equilibrium state, much larger than the 30 hours in the trial section. The results suggested that rainfall had a detrimental effect on the drying of BE-CIR pavement. If it was rainy at the end of construction, the timing of overlay placement should be delayed to ensure the drying of the BE-CIR layer.

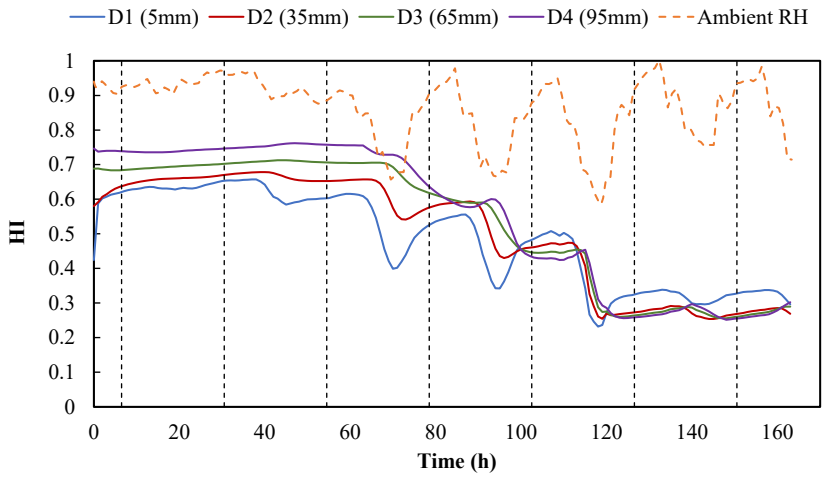

Fig. 17. HI calculation results for condition 1.

Fig. 18 illustrates the result of HI calculation of the BE-CIR layer for condition 2. From 0 to the 50th hour, the HI at each depth decreased with the ambient RH fluctuation. The rate of decrease was faster in the 40th to the 50th hour than in the 0 to the 40th hour. After the 50th hour, the overall HI at all depths stabilized at about 0.3. From the 50th to the 90th hour, the HI of BE-CIR increased slightly corresponding to the overall increase in ambient RH. After 90 hours, the BE-CIR dryness declined with the overall decrease in ambient RH. The results suggested that for the condition 2, representing low-temperature normal days, 50 curing hours were required to reach the moisture equilibrium state for the BE-CIR layer. The drying time for condition 2 was longer than that measured in the trial section with high temperature and low humidity due to the reduction of the effective diffusion coefficient caused by temperature drop. However, the drying time for condition 2 was shorter than that for condition 1, which was a rainy day after compaction.

The simulation results of the two working conditions indicated that the curing environment after compaction could significantly affect the drying behavior of the BE-CIR layer, mainly in terms of the time duration of curing to the moisture equilibrium state as influenced by ambient temperature and RH.

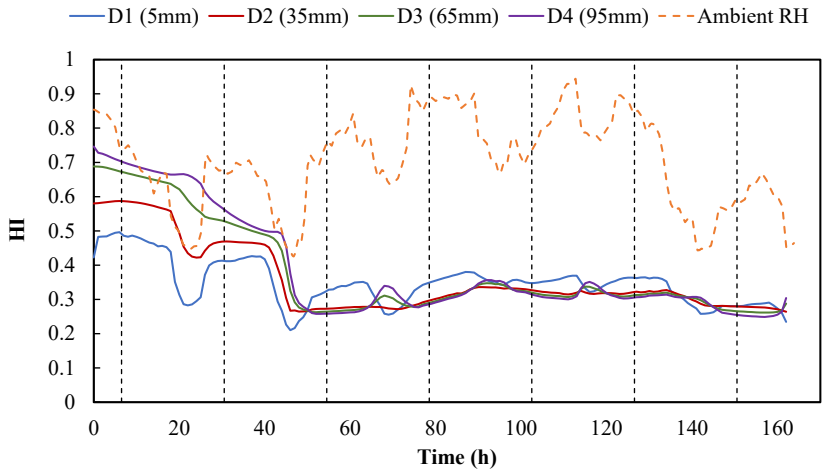

Fig. 18. HI calculation results for condition 2.

4 CONCLUSIONS

In this research, drying behavior models of BE-CIR were developed for laboratory mixture and field pavement, respectively. Heat-moisture coupling effect was considered to ensure the modeling accuracy. A model of laboratory mixture was established, and the model parameters were calibrated by comparing the simulation results with the measured data. A field pavement model was developed based on actual environmental conditions, corrected material parameters, and pavement structural layer information. Monitoring data obtained from the sensors were used to define the initial temperature and humidity conditions and to validate the simulation. The validated model simulated the pavement drying behavior under two natural curing environments different from the field pavement. The calculations could provide a guide to the curing duration before overlay placement in different natural environments. A complete process of model establishment, parameters calibration, model validation, and model application of BE-CIR pavement drying behavior was determined. The primary results and conclusions can be summarized as follows:

(1) A time-variable coefficient was introduced for the unique strength formation process of BE-CIR. Laboratory model calculations showed that water loss in the first three curing days was much less than the measured value, indicating that the effective diffusion coefficient of BE-CIR was not a constant value but decreased with the strength formation during the curing process. Based on laboratory test results, relationships between several physical parameters were established to determine the form of the time-variable coefficient and fitting parameters.

(2) A depth correction coefficient was introduced to characterize the unidirectional moisture evaporation of BE-CIR. Mixture model calculations corrected by the time-variable coefficient indicated that the moisture gradient distribution pattern in depth was inconsistent with the measurements. The depth correction coefficient was proposed by combining the relationship between moisture evaporation, strength formation, and effective diffusion coefficient.

(3) With testing of the BE-CIR mixture's basic material parameters after curing and the introduction of two correction coefficients, the pavement model with insulation on the sides and bottom can accurately predict the drying behavior of BE-CIR pavements under the heat-moisture coupling effects. The gradient characteristics and variation patterns of the temperature and moisture fields of the BE-CIR pavement under natural curing environments were precisely calculated.

(4) Curing environments with low temperatures and high humidity extended the time it took to reach moisture equilibrium for the BE-CIR pavement, implying a delay in overlay placement. The curing time to moisture equilibrium was calculated to be 120 hours for condition 1, representing medium temperature and high humidity, 50 hours for condition 2, representing low temperature and medium humidity, and greater than 30 hours for the trial section, representing high temperature and low humidity.

Based on the finite element model proposed in this research, it is necessary to establish a strength prediction model for BE-CIR pavement in the future to calculate the al mechanical response under the multi-physical field coupling effects. This appears to have a significant potential to study the development and deterioration mechanisms of BE-CIR material properties under complex curing conditions and to establish a real-time responsive digital twin model.

ACKNOWLEDGMENTS

This work was supported by the National Natural Science Foundation of China (Grant No. 52108421) and the Hong Kong Research Grant Council through the GRF project (Grant No. 15220621).

REFERENCES

Alkins, A.E., Lane, B., Kazmierowski, T., 2008. Sustainable Pavements: Environmental, Economic, and Social Benefits of In Situ Pavement Recycling. Transportation Research Record 2084, 100–103. https://doi.org/10.3141/2084-11

Apeagyei, A.K., Grenfell, J.R.A., Airey, G.D., 2015. Application of Fickian and non-Fickian diffusion models to study moisture diffusion in asphalt mastics. Mater Struct 48, 1461–1474. https://doi.org/10.1617/s11527-014-0246-2

Apeagyei, A.K., Grenfell, J.R.A., Airey, G.D., 2014. Evaluation of Moisture Sorption and Diffusion Characteristics of Asphalt Mastics Using Manual and Automated Gravimetric Sorption Techniques. J Mater Civil Eng 26, 04014045. https://doi.org/10.1061/(ASCE)MT.1943-5533.0000929

Arambula, E., Caro, S., Masad, E., 2010. Experimental Measurement and Numerical Simulation of Water Vapor Diffusion through Asphalt Pavement Materials. J Mater Civil Eng 22, 588–598. https://doi.org/10.1061/(ASCE)MT.1943-5533.0000059

ASTM, 2014. Standard Test Methods for Gravimetric Determination of Water Vapor Transmission Rate of Materials, E96/E96M16.

Du, S., 2014. Interaction mechanism of cement and asphalt emulsion in asphalt emulsion mixtures. Mater Struct 47, 1149–1159. https://doi.org/10.1617/s11527-013-0118-1

Flores, G., Gallego, J., Miranda, L., Marcobal, J.R., 2020. Cold asphalt mix with emulsion and 100% rap: Compaction energy and influence of emulsion and cement content. Construction and Building Materials 250, 118804. https://doi.org/10.1016/j.conbuildmat.2020.118804

Gao, L., Ni, F., Charmot, S., Luo, H., 2014. Influence on Compaction of Cold Recycled Mixes with Emulsions Using the Superpave Gyratory Compaction. J. Mater. Civ. Eng. 26, 04014081. https://doi.org/10.1061/(ASCE)MT.1943-5533.0000987

Graziani, A., Godenzoni, C., Cardone, F., Bocci, M., 2016. Effect of curing on the physical and mechanical properties of cold-recycled bituminous mixtures. Mater. Des. 95, 358–369. https://doi.org/10.1016/j.matdes.2016.01.094

Graziani, A., Iafelice, C., Raschia, S., Perraton, D., Carter, A., 2018. A procedure for characterizing the curing process of cold recycled bitumen emulsion mixtures. Constr Build Mater 173, 754–762. https://doi.org/10.1016/j.conbuildmat.2018.04.091

Gu, F., Ma, W., West, R.C., Taylor, A.J., Zhang, Y., 2019. Structural performance and sustainability assessment of cold central-plant and in-place recycled asphalt pavements: A case study. Journal of Cleaner Production 208, 1513–1523. https://doi.org/10.1016/j.jclepro.2018.10.222

Jiang, J., Zhao, Z., Jiang, X., Leng, Z., Yang, B., Ni, F., 2023. Moisture migration characterization of bitumen emulsion-based cold in-place recycling mixture over curing. Mater Struct 56, 122. https://doi.org/10.1617/s11527-023-02212-x

Khan, A., Redelius, P., Kringos, N., 2016. Toward a new experimental method for measuring coalescence in bitumen emulsions: A study of two bitumen droplets. Colloids and Surfaces A: Physicochemical and Engineering Aspects 494, 228–240. https://doi.org/10.1016/j.colsurfa.2016.01.045

Kim, Y.-J., Lee, H.-S.D., Im, S.-H., 2011. Development of Moisture Loss Index Based on Field Moisture Measurement using Portable Time Domain Reflectometer (TDR) for Cold In-place Recycled Pavements. Journal of the Korean Society of Road Engineers 13, 139–145. https://doi.org/10.7855/IJHE.2011.13.2.139

M. L. Hoang, P. Verboven, M. Baelmans, B. M. Nicolaï, 2003. A CONTINUUM MODEL FOR AIRFLOW, HEAT AND MASS TRANSFER IN BULK OF CHICORY ROOTS. Transactions of the ASAE 46, 1603–1611. https://doi.org/10.13031/2013.15623

Ma, L., Varveri, A., Jing, R., Kasbergen, C., Erkens, S., 2022. Thermodynamics and kinetics of moisture transport in bitumen. Mater Design 222, 111028. https://doi.org/10.1016/j.matdes.2022.111028

Miljković, M., Radenberg, M., 2015. Characterising the influence of bitumen emulsion on asphalt mixture performance. Mater Struct 48, 2195–2210. https://doi.org/10.1617/s11527-014-0302-y

Modarres, A., Rahimzadeh, M., Zarrabi, M., 2014. Field investigation of pavement rehabilitation utilizing cold in-place recycling. Resources, Conservation and Recycling 83, 112–120. https://doi.org/10.1016/j.resconrec.2013.12.011

MOT, 2019. Technical Specifications for Highway Asphalt Pavement Recycling (in Chinese). Ministry of Transport of the People's Republic of China. JTG/T 5521–2019.

Nuijten, A.D.W., Høyland, K.V., 2017. Modelling the thermal conductivity of a melting snow layer on a heated pavement. Cold Regions Science and Technology 140, 20–29. https://doi.org/10.1016/j.coldregions.2017.04.008

Ogbo, C., Dave, E.V., Sias, J.E., Zegeye, E., 2022. Correlating field and laboratory evolution of curing in cold in-place recycled (CIR) materials. Constr Build Mater 345, 128352. https://doi.org/10.1016/j.conbuildmat.2022.128352

Ouyang, J., Pan, B., Xu, W., Hu, L., 2019. Effect of Water Content on Volumetric and Mechanical Properties of Cement Bitumen Emulsion Mixture. Journal of Materials in Civil Engineering 31, 04019085. https://doi.org/10.1061/(ASCE)MT.1943-5533.0002736

Paul, A., Laurila, T., Vuorinen, V., Divinski, S.V., 2014. Fick's Laws of Diffusion, in: Paul, A., Laurila, T., Vuorinen, V., Divinski, S.V. (Eds.), Thermodynamics, Diffusion and the Kirkendall Effect in Solids. Springer International Publishing, Cham, pp. 115–139. https://doi.org/10.1007/978-3-319-07461-0_3

Saadoon, T., Garcia, A., Gómez-Meijide, B., 2017. Dynamics of water evaporation in cold asphalt mixtures. Mater Design 134, 196–206. https://doi.org/10.1016/j.matdes.2017.08.040

Sun, T., Sheng, H., 2020. Multi-physical field study of asphalt mixtures containing moisture based on microwave heating. J Microwave Power Ee 54, 35–51. https://doi.org/10.1080/08327823.2020.1714105

Welty, J.R., Wicks, C.E., Wilson, R.E., 1976. Fundamentals of Momentum, Heat, and Mass Transfer. Wiley.

Winterton, R.H.S., 1999. Newton's law of cooling. Contemporary Physics 40, 205–212. https://doi.org/10.1080/001075199181549

Xiao, F., Yao, S., Wang, J., Li, X., Amirkhanian, S., 2018. A literature review on cold recycling technology of asphalt pavement. Construction and Building Materials 180, 579–604. https://doi.org/10.1016/j.conbuildmat.2018.06.006

Zhao, Z., Jiang, J., Chen, Z., Ni, F., 2022. Moisture migration of bitumen emulsion-based cold in-place recycling pavement after compaction: Real-time field measurement and laboratory investigation. J Clean Prod 360, 132213. https://doi.org/10.1016/j.jclepro.2022.132213

Zhao, Z., Ni, F., Zheng, J., Cheng, Z., Xie, S., 2023. Evaluation of Curing Effects on Bitumen Emulsion-Based Cold In-Place Recycling Mixture Considering Field-Water Evaporation and Heat-Transfer Conditions. Coatings 13, 1204. https://doi.org/10.3390/coatings13071204